MICROSTRUCTURE AND STRENGTH OF THE BOND BETWEEN CONCRETE AND STYRENE-BUTADIENE LATEX-MODIFIED MORTAR

J. E. Isenburg and D. E. Rapp,
The Dow Chemical Company, Midland, Michigan;
E. J. Sutton,* City of Midland; and
J. W. Vanderhoff,* Lehigh University, Bethlehem, Pennsylvania

Various surface preparations were used in resurfacing concrete with a latex-modified mortar. A 1-in. mortar cap was applied to the circular surface of 14-day old, high early strength concrete cylinders treated in various ways. After aging 14 days, several cylinders of each group were fractured in a shear bond test, and an unfractured cylinder was sawed to provide a ½-in. cube that included the interface between concrete and mortar. These cubes were fractured normal to the interface, producing a surface free of sawing artifacts. After they were examined in the scanning electron microscope, these sections were fractured again to simulate the shear bond test and then reexamined. Several performance variations are explained by the scanning electron photographs.

•CONSIDERABLE RESEARCH EFFORTS for the past 15 years have been devoted to the use of styrene-butadiene and vinylidene chloride copolymer latexes in the modification of portland cement systems. These materials have been used to resurface old concrete floors, roads, and bridges where the bond strength of a thin-mortar overlay is extremely important (1, 2). The purpose of this study is to show the effect of various parameters on the physical properties and morphology of styrene-butadiene latex-modified mortar overlays on aged concrete substrates, i.e., to reproduce in the laboratory the various methods of resurfacing the deteriorated surfaces of concrete highways and bridge decks and to compare these methods according to the shear bond strength and morphology of the composite. The parameters studied were the various techniques for the preparation of the concrete substrate surface and for the application of the latex-modified mortar to this substrate.

SHEAR BOND STRENGTH TESTS

Preparation of Specimens

The mix used for the concrete substrates is given in Table 1. The substrates were prepared in the form of cylinders (3.4 in. diameter, 6.5 in. height) by casting the mix in a cardboard carton. The circular top surface was finished by troweling, and the cylinders were cured under wet towels for 24 hours at room temperature. The cartons were then cut away, and the concrete cylinders were placed upright on the troweled ends and were cured in a fog room for 13 days at 73 F and 100 percent relative humidity (RH). The compressive strengths of these cylinders at 7 and 14 days were about 5,000 and 6,000 psi respectively.

*When this research was performed, Messrs. Sutton and Vanderhoff were with The Dow Chemical Company.

Sponsored by Committee on Basic Research Pertaining to Portland Cement and Concrete.

TABLE 1
CONCRETE SUBSTRATE MIX

Component	Parts by Weight
Crushed dolomitic limestone, 25A[a]	293
Natural sand, 2NS[a]	200
High early strength portland cement	100
Water	61.4
Total	654.4
Compressive strength of 4- by 8-in. cylinders, psi	
14 days	6,070
28 days	6,530

[a]The aggregates meet the designated specifications of the Michigan Department of State Highways.

TABLE 2
MORTAR OVERLAY MIXES

Component	Parts by Weight	
	Overlay Containing Latex	Control Overlay
Natural sand, 2NS	324	324
Styrene-butadiene copolymer latex, 48 percent solids	31	—
High early strength portland cement	100	100
Water	21.4	61.4
Total	476.4	485.4
Air content, percent[a]	8.0	8.8
Compressive strength of 4- by 8-in. cylinders, psi		
14 days	5,150	6,010
28 days	5,350	5,900

[a]ASTM Method C 185-59 (Standard Method of Test for Air Content of Hydraulic Cement Mortar).

The mixes used for the overlays are given in Table 2. The concrete cylinders that had aged for 14 days were removed from the fog room and the troweled ends were sandblasted to prepare the surface for the application of the overlay. Then a section of another carton was taped around the sandblasted end, forming a cylindrical mold with the top 1 in. above the sandblasted surface. The surface was wet, a thin layer of the latex-modified mortar was brushed into it to ensure good contact, and then the rest was added and tamped in. Finally, the top was struck to form a 1-in. thick mortar layer. The composite was damp-cured for 24 hours and was then cured for 14 days at 73 F and 50 percent RH. In addition, 7 variations of this standard sample were prepared: composite was aged 7 instead of 14 days before testing; composite was aged 3 days before testing; overlay was "vibrated on" the substrate instead of being brushed and tamped; substrate was a 2-year-old specimen taken from a road; substrate was sandblasted but not wet; substrate was wet but not sandblasted; and overlay was of control mortar mixture without latex.

The control mortar overlay was damp-cured for 24 hours and then for 14 days at 100 percent RH in a fog room. Five specimens were prepared for each variation. After the appropriate aging time, four of these were fractured in the shear bond strength test, and the fifth specimen was sectioned and examined by scanning electron microscopy.

TABLE 3
SHEAR BOND STRENGTH

Sample	Shear Bond Strength, psi[a]	Probability That Strength of Standard Sample Is Greater
Standard	474	—
Composite		
Aged 7 days	391	97
Aged 3 days	319	99
Overlay vibrated on	418	90
Two-year-old concrete substrate	428	69
Substrate not wet	528	—[b]
Substrate not sandblasted	385	94
Control (without latex)	249	99 —[c]

[a]Average of 3 specimens for 2-year substrate; average of 4 specimens for all others.
[b]Because 528 ⟩ 474, probability that substrate not wet ⟩ standard = 90 percent.
[c]Also probability that 7-day composite ⟩ 3-day composite = 94 percent and probability that 2-year substrate ⟩ control = 97 percent.

Shear Bond Strength Test Results

After aging, the cylinders were tested in shear bond (1). Observations were made of the mode of fracture, i.e., through the overlay or through the substrate. The average values of the shear bond strengths are given in Table 3. In general, the shear bond strengths of the latex-modified mortar are nearly twice as great as that of the control mortar.

Statistical Analysis of Results

These averages are derived from the results of only 4 tests, which showed some experimental scatter. The usual methods of statistical analysis are not applicable in this case because of the small number of specimens and the expectation that the statistical distribution of test results are not necessarily a normal distribution.

Therefore, these data were analyzed by the Wilcoxon Test (3), which was developed to treat cases of this kind. As an example of the Wilcoxon Test, the following comparison between the standard sample and the 7-day composite sample gives individual values of the shear bond strength of each sample ranked in decreasing order: standard—508, 496, 478, and 413 psi; and 7-day composite—418, 404, 379, and 364 psi. These values are then combined and ranked according to the highest, second-highest, third-highest, and so forth: standard—1st, 2nd, 3rd, 5th, sum 11; and 7-day composite—4th, 6th, 7th, 8th, sum 25.

The disparity between the preceding sums is 25 - 11, or 14. From the tables given in Siegal's Study (3), the probability is only 0.029 that a disparity equal to or greater than this value will occur as a random variation. The results of these comparisons are given in the last column of Table 3. The data given in Table 3 show that the shear bond strength increased progressively with aging times of 3, 7, and 14 days. This was corroborated by the mode of fracture: completely at the interface in the 3-day samples; entirely through the substrate at some distance from the interface in the 14-day samples. Also, the brushing technique in the latex-modified mortar gave higher strengths than the vibrating technique. For the surface preparation, the unwet but sandblasted sample displayed higher strengths than the wet and sandblasted sample, which in turn displayed higher strengths than the wet but not sandblasted sample. In all comparisons, the shear bond strengths of the latex-modified samples were significantly greater than those of the control sample. The only comparison of doubtful significance was that between the standard and the 2-year-old concrete substrate samples; however, the latter sample had only 3 specimens, with considerable experimental scatter.

SCANNING ELECTRON MICROSCOPY

Preparation of the Specimens

For examination in the scanning electron microscope (4), the fifth (untested) cylindrical specimen of each sample was sectioned with a diamond saw to produce a ½-in. cube, which contained almost equal amounts of the overlay and the substrate. This cube was fractured perpendicularly to the interface to produce two ¼-in. slabs, each showing an interior fracture surface spanning the interface between the overlay and the substrate. This ¼-in. slab was positioned on the sample mounting stub, coated under vacuum with evaporated gold, and examined in the Stereoscan Mark IIa scanning electron microscope. (This equipment is manufactured by the Cambridge Instrument Company, England, and is distributed by Kent Cambridge Scientific, Inc., Morton Grove, Illinois.) In some cases, color optical photomicrographs were made before the slabs were metalized, so that, when the sample was examined in the scanning electron microscope, the interface could be located and the various types of particles—limestone and sand grains—could be identified by their color, luster, and texture.

For some microscope specimens, the shear bond strength test was simulated by removing the ¼-in. slab from the mounting stub after examination, clamping the concrete end in a vise with the interface aligned with the lips, and pushing on the protruding end until it fractured. The 2 pieces were then remounted on the stub so that the salient features of the morphology of the interface could be compared. Qualitatively, the results correlated with the shear bond strength tests. Those specimens that fractured through the interface in the shear bond strength test usually gave clean fractures through the interface in the microscope samples. Also, those stronger samples that fractured through the concrete substrate usually did so in both cases.

Results of Scanning Electron Microscopy

Let us first consider the particle size and expected appearance of the ingredients used. The 25A crushed dolomitic limestone contains particles in the size range of 0.09 to 0.5 in. (2.4 to 13 mm). The 2NS natural sand passes a No. 4 sieve and is retained on a No. 100 sieve, which corresponds to the size range of 0.006 to 0.2 in. (0.15 to 4.8 mm). The average particle size of the latex is about 0.2 μm (0.0002 mm), and its particle size distribution is relatively narrow. Because the scanning electron

microscope offers a wide range of magnifications, a relatively large area (about 3 mm square) of each specimen was examined first at low magnification. Under these conditions, the limestone and sand grains could be identified easily by their shape or by reference to the optical color photomicrographs. Moreover, in most cases, the interface between the overlay and the substrate could be located precisely. Then, specific features of the morphology in this region thought to be of interest were examined in greater detail by increasing the magnification in regular steps to a much higher value. The morphology of the cement grains was altered by the hydration reactions, and the various crystalline forms observed are described in the following sections. The very small latex particles are perfect spheres in the mortar mix, but when dry the particles coalesce to form a continuous film in which the individual particles lose their identity. Therefore, the latex polymer would be expected to form an amorphous mass of coalesced particles having no distinguishing morphological characteristics.

The first sample described is the control mortar overlay (without latex) on the concrete substrate. Figures 1, 2, 3, and 4 show several series at increasing magnification; all except Figure 1a are scanning electron micrographs. The first series shows a fracture surface that is perpendicular to the overlay-substrate interface. In each micrograph, the interface is marked with arrows labeled I, and the area to be shown at higher magnification in the next micrograph is outlined by the corners; e.g., the outlined area shown in Figure 1b is the subject of Figure 1c. Figure 1a is a black and white copy of a color optical photomicrograph of the specimen before it was metalized. The interface could be seen clearly in the color photograph and was then marked as I

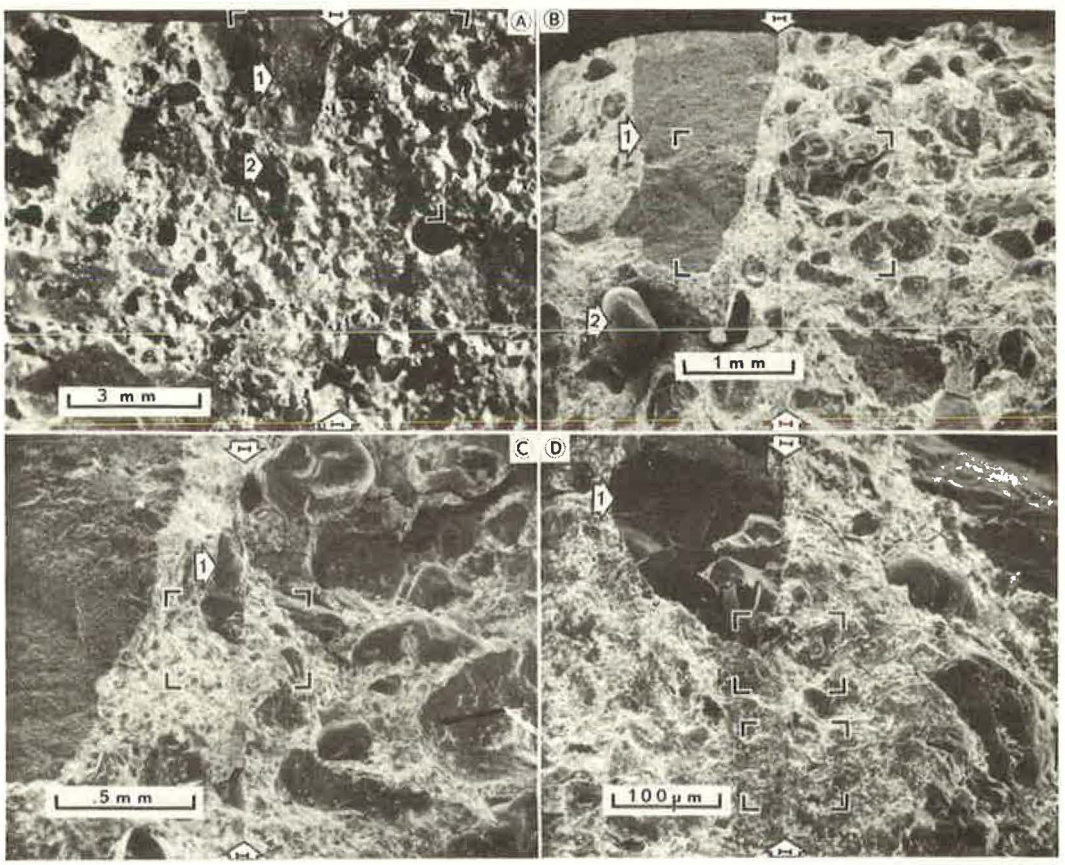

Figure 1. Control sample: overlay substrate interface.

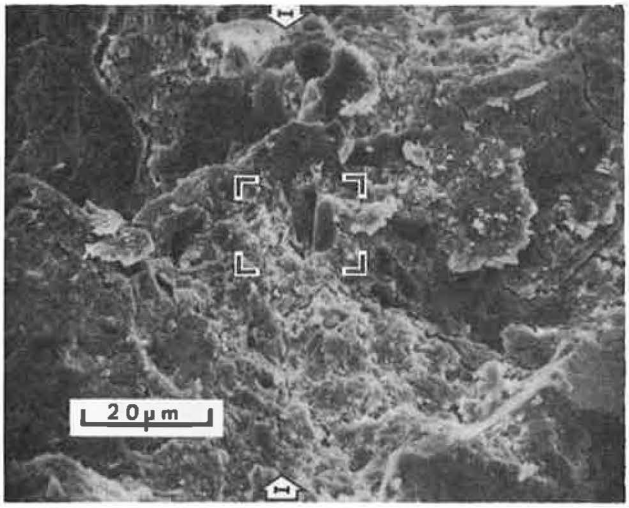

Figure 2a

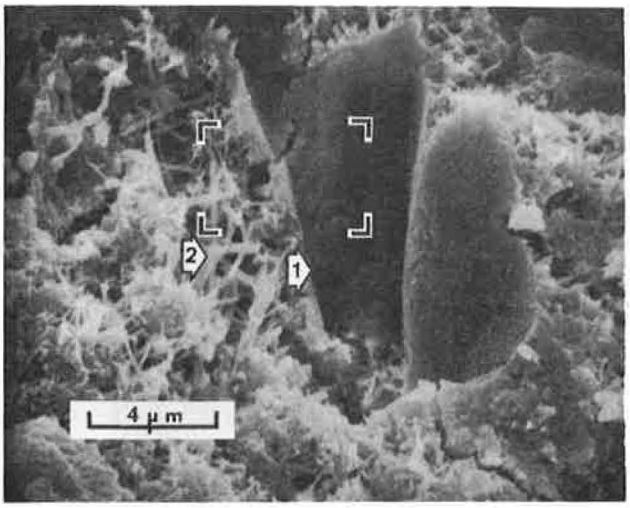

Figure 2b

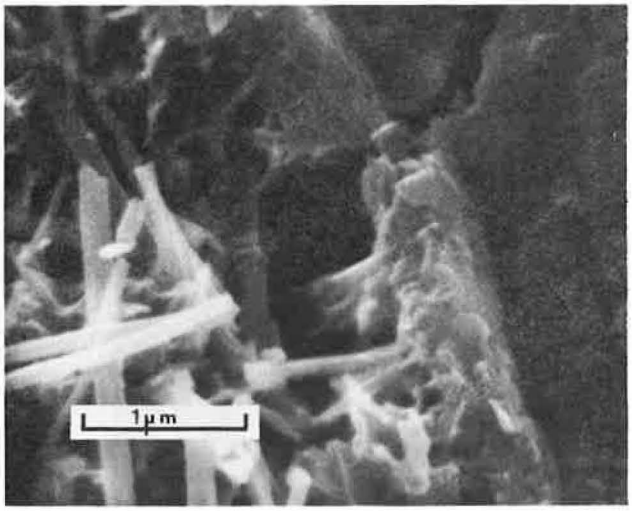

Figure 2c

Figure 2. Control sample: upper outlined area in Figure 1d.

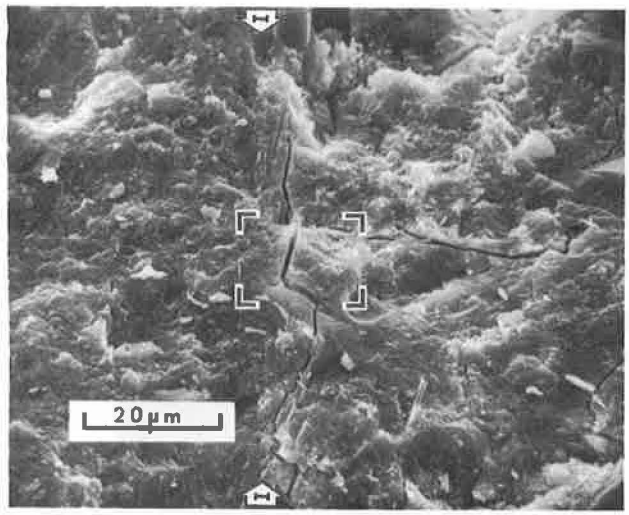

Figure 3a

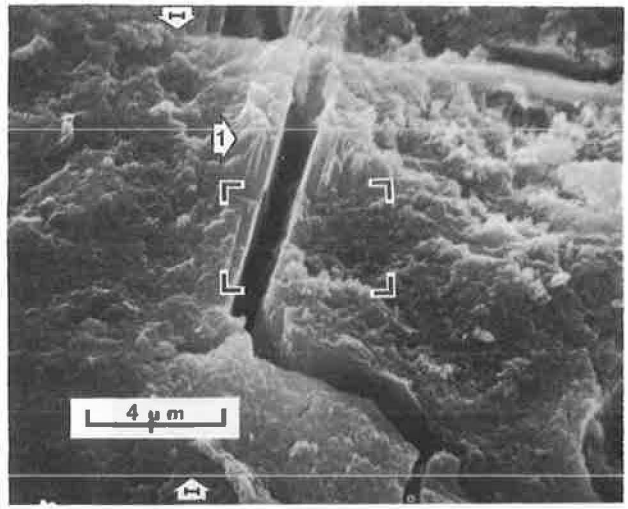

Figure 3b

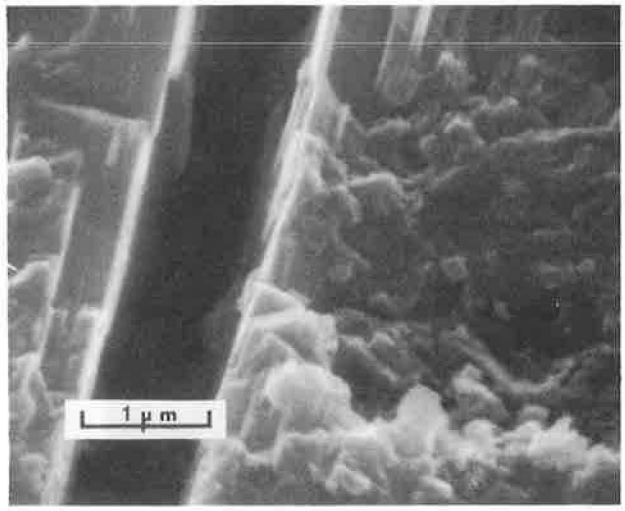

Figure 3c

Figure 3. Control sample: lower outlined area in Figure 1d.

on the black and white copy. The overlay is to the right and the substrate is to the left. A limestone grain (arrow 1) and a silica sand grain (arrow 2) can be identified in the substrate. A comparison of Figures 1a and 1b shows that the outlines of the limestone grain are shown much more clearly by scanning electron microscopy than by optical microscopy. For the silica sand grain, however, the luster and transparency that serve to identify it can be seen only in the optical photomicrograph. The sawed edge of the ½-in. cube can be seen at the top of both figures. The great depth of field of the scanning electron microscope is shown in Figure 1b; the specimen was tilted at an angle of 45 deg to the electron beam, yet almost all of it is in sharp focus.

Figures 1c and 1d show that the overlay-substrate interface is still apparent at higher magnification. Also, a sand grain flush with the surface of the substrate (arrow 1) can be seen in contact with the overlay.

The 2 areas outlined in Figure 1d are shown at higher magnification in Figures 2 and 3; the upper area is shown in Figures 2a, 2b, and 2c and the lower area is shown in Figures 3a, 3b, and 3c. Figures 2a and 3a show that the interface is less distinct at this higher magnification. Both figures show an extensive network of microcracks, which seem characteristic of the control mortar overlay near the interface. Figure 2b shows that the interface can no longer be distinguished and that the microstructure is characteristic of that of portland cement mortar observed at early aging times. One such feature is the layer of hydration products deposited on the surface of the sand grains; e.g., a sand grain was extracted by the fracturing, leaving a smooth imprint (arrow 1). It is also characteristic that the channels between the sand and cement grains are filled with a network of needle-like crystals (arrow 2). The needles and sand grain imprints are shown at higher magnification in Figure 2c. Figures 3a, 3b, and 3c show the microcrack structure of the overlay immediately adjacent to the interface. The fact that the periodic straight cracks are slanted at the same angle suggests that they are the result of cleavage of crystal masses lying along the interface. As shown in Figure 3b, the interface is believed to lie between the I arrows, and arrow 1 shows a structure interpreted as a crystal mass. The width of the microcrack shown in Figure 3c is 0.9 to 1.1 μm. Such microcracks must certainly indicate a point of weakness in the adhesion of the overlay to the substrate.

The 1/2-in. cube specimen was removed from the mounting stub and was fractured again to simulate the shear bond strength test. This new fracture provided a good example of failure at the interface. The specimen was remounted so as to expose the new fracture surface—the interface itself. Thus, Figure 4 shows micrographs of the overlay side of the interface exposed by the shear bond test. In Figure 4a, the edge of the specimen on the left side is part of the fracture surface shown in Figures 1, 2, and 3. The smooth area in the center is where the mortar was in contact with a limestone grain that was removed by the fracture, taking fragments of mortar with it and leaving the fragments of limestone. This was confirmed by examination of the limestone grain itself in the "mate" of the specimen. Figure 4b shows a hole left by the removal of a mortar fragment (arrow 1) and a fragment of limestone still adhering to the mortar (arrow 2). Figure 4c shows, however, that this fracture is not an ideal example of interfacial failure; actually, the failure occurred irregularly on both sides of the interface between the overlay and the substrate. Figure 4d shows irregular fractures through the mortar side of the interface. These fractures exposed channels between sand and cement grains similar to those shown in Figure 2b. These channels were also filled with networks of needle-like crystals (arrow 1). The needles are shown in greater detail in Figures 4e and 4f. In Figure 4f, the parallel striations along the axis of the needles are less than 0.05 μm (500 Å) apart, exemplifying the best resolution obtained to date with our scanning electron microscope.

Thus, Figures 1, 2, 3, and 4 show the following characteristics of the microstructure of the control mortar overlay on a concrete substrate after aging 28 days:

1. The open channels between the sand and cement grains are filled with networks of needle-like crystals;
2. The surfaces of the sand grains are covered with a layered deposit;
3. The overlay is veined with microcracks, some of which follow the overlay-substrate interface for a distance; and

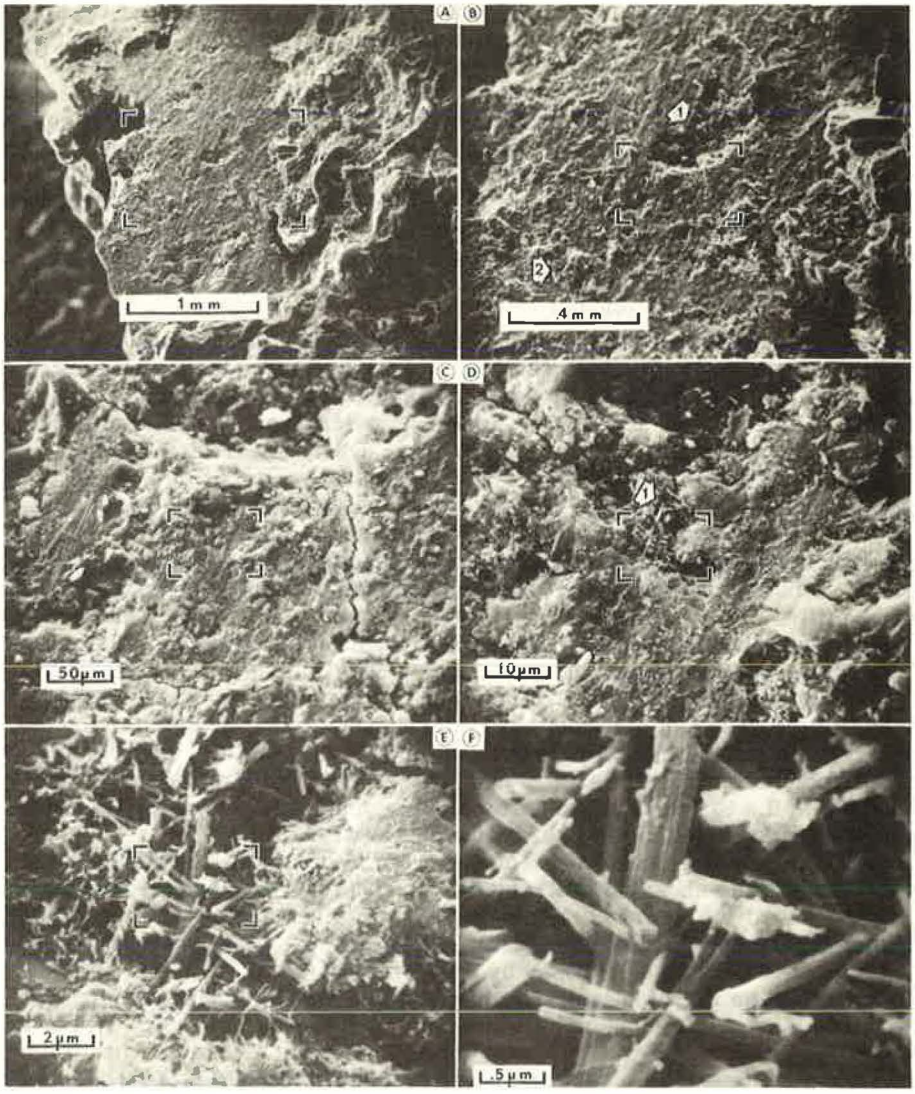

Figure 4. Control sample: overlay side of shear bond fracture.

4. The shear bond test fracture generally follows the interface, but sometimes it passes through weak areas on either side of it.

The technique of examining the samples fractured perpendicularly to the interface, fracturing them again to simulate the shear bond strength test, and then examining the mated interfaces generated by this new fracture has been applied to the other samples of this study. To date, more than 250 electron micrographs of these specimens have been examined. Space permits us to show only a few of the micrographs that demonstrate the usefulness of this technique in explaining the results of the shear bond strength tests.

It was shown previously that the shear bond strength of the latex-containing overlay was lower when the concrete substrate was not sandblasted. Figures 5, 6, and 7 show an explanation for this result. Figure 5 shows the overlay-substrate interface for the standard latex-containing mortar and the unsandblasted concrete substrate. In Figure 5a, the interface marked with the arrows I runs from the lower left to the upper

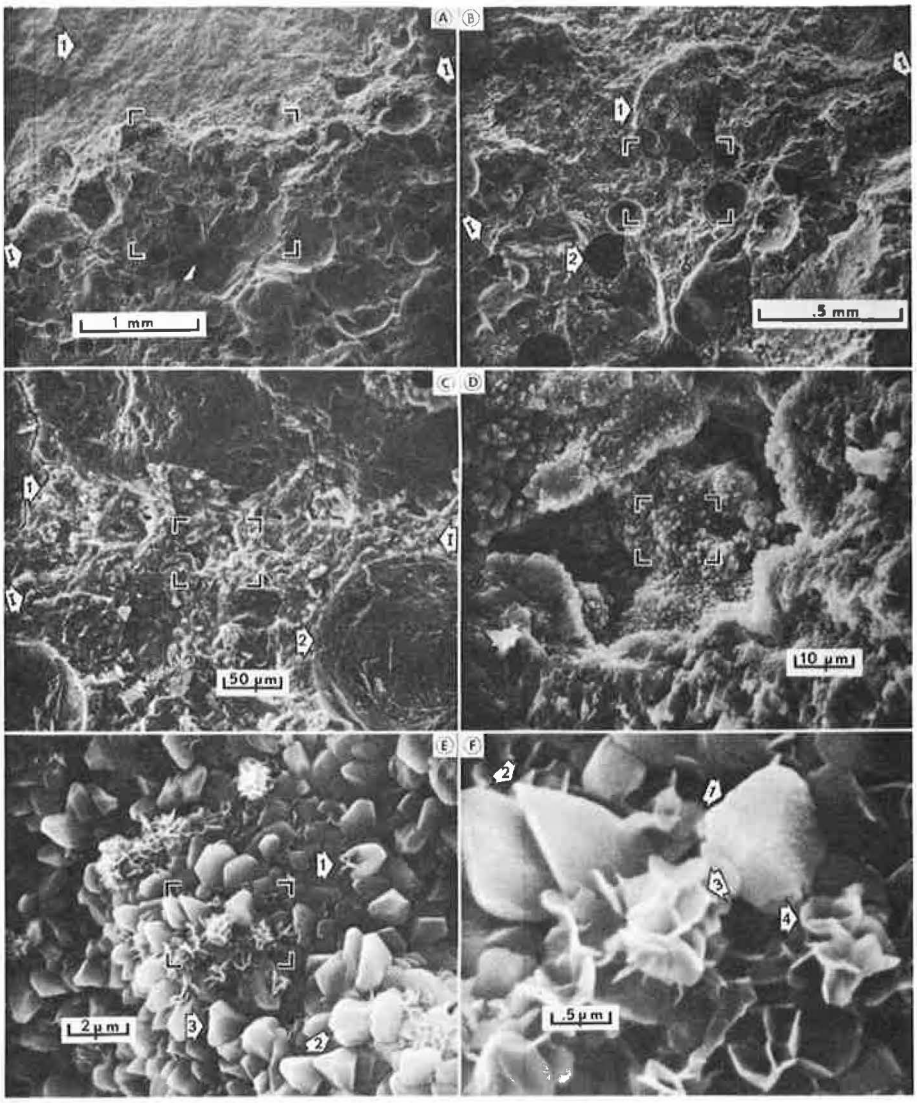

Figure 5. Standard unsandblasted sample: overlay-substrate interface.

right, with the substrate to the left and the overlay to the right. Note the limestone grain (arrow 1) in the substrate less than 1 mm from the interface. Figure 5b shows a sand grain (arrow 1) in the substrate near the interface and several bubble holes in the overlay (arrow 2). These holes are attributed to entrained air bubbles; evidently the fracture plane intersected the bubble hole, revealing it to be a hollow sphere. This interpretation is supported by the presence inside the hole of crystal growths, which are apparently hydration products. Figure 5c shows a string of tiny open pockets along the interface. Inside these is a 10-μm to 100-μm thick layer of material, extending from the interface to arrow 1. Figure 5c also shows the crystals that have grown in the bubble holes (arrow 2). Figure 5d shows that the crystals lining one of the larger pockets are of 2 types; leaf-shaped and granular. Details of the crystal habit of these 2 forms are pointed out in Figures 5e and 5f. These open pockets lined with crystals follow the interface just below the surface of the concrete substrate.

The question as to the prevalence of these pockets is answered by examination of the surface after shear bond fracture. In this case, the failure was judged visually to be present entirely throughout the interface. Figure 6 shows the concrete substrate side of the shear bond fracture specimen. Even at the lowest magnification (Fig. 6a), the failure does not appear to be entirely at the interface. There are plateaus of the original interface interspersed with fuzzy areas and exposed sand grain surfaces, which must have been below the original interface. Figure 6b shows a plateau of the original interface (arrow 1) at higher magnification as well as the perimeter of a fuzzy area (arrow 2) and a deep fracture exposing a sand grain (arrow 3). Figure 6c shows that the fuzzy area is actually a myriad of crystals extending through veins and fissures across the fracture surface. The vein of needle-like crystals (lower framed area) is shown at higher magnification in Figure 6d. Stereoscopic observation of this field confirmed that the needles spanned the vein, because their ends (arrow 1) had been broken off and the mass (arrow 2) is much lower than the surface in the lower right corner to

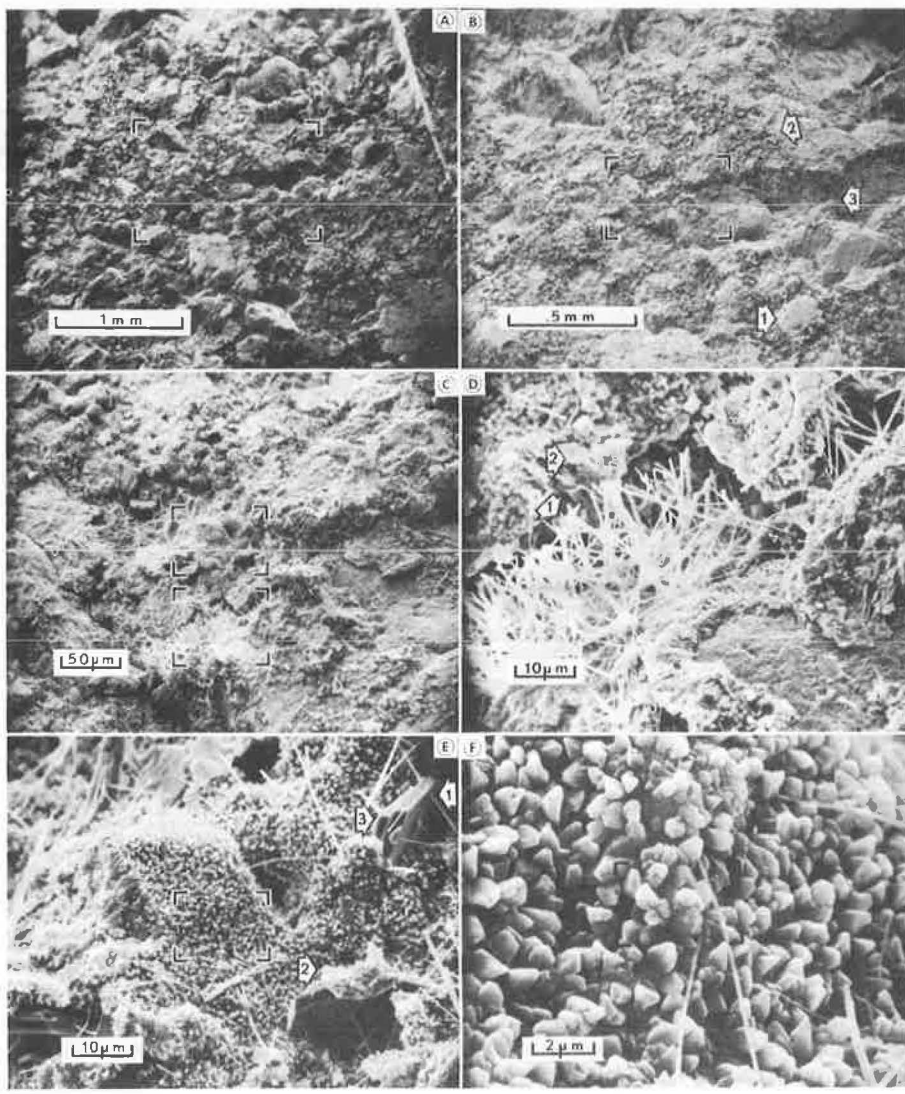

Figure 6. Standard unsandblasted sample: substrate side of shear bond fracture.

which the needles are attached. Figures 6e and 6f show the intercrystallization of several crystal forms; e.g., in one case (Fig. 6e), a needle penetrated a plate (arrow 1). In the lower right corner (Fig. 6e), a piece of amorphous material, probably the original roof of the pocket, is still adhering to a plate (arrow 2). Note the slanted edges of the large plates (arrow 3). Stereoscopic observation suggests that the orientation of these edges is rhombohedral; the crystal form of the tabular plates would then be rhombohedral pinacoids. The granular crystals shown in the background of Figure 6e are of the same size and crystal habit as those shown in Figure 5f; however, in the present case, there are no masses of tiny leaf-shaped crystals. Such observations on crystal morphology will eventually lead us to the identification of these crystals.

Thus, it appears that the pockets lined with crystals are actually "caverns" that extend parallel to the interface for relatively great distances and that constitute a significant proportion of the interfacial area. This is verified by Figures 7a and 7b,

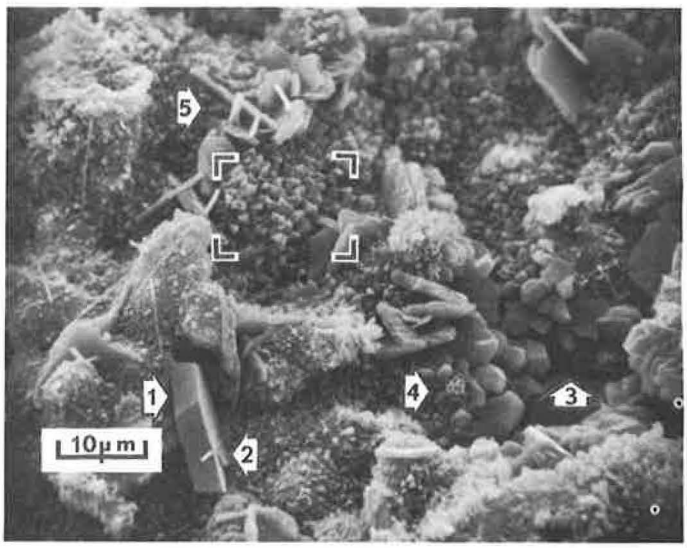

Figure 7a

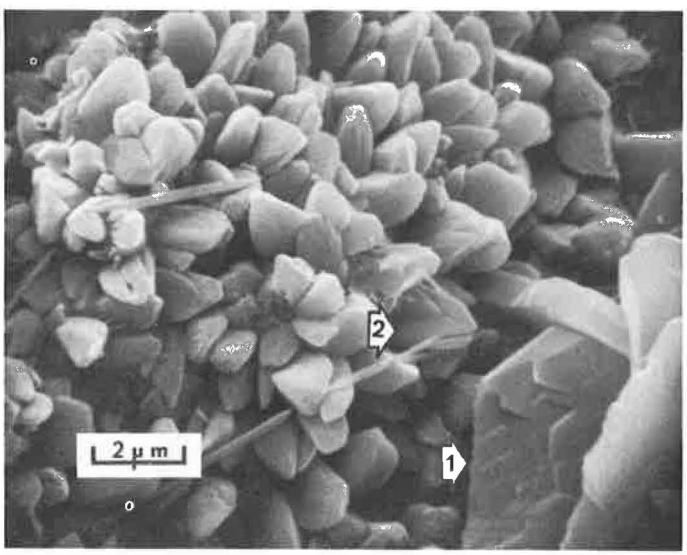

Figure 7b

Figure 7. Standard unsandblasted sample: overlay side of shear bond fracture.

which show the mortar side of the fracture surface corresponding to the substrate shown in Figure 6 (i.e., the roof of the cavern that was split apart by the shear bond fracture). Figure 7a is remarkable in that it shows 5 different crystal shapes, all growing together and lining the roof of the cavern. One large plate (arrow 1) in the form of a rhombohedral pinacoid has a needle (arrow 2) growing out of it. Also seen are the granular ground mass (arrow 3) with its pyramidal shape and the accompanying tiny, twinned, leaf-shaped crystals (arrow 4). Finally, there is a new type of plate crystal (arrow 5), as shown in Figure 7b that is terminated by a series of hexagonal steps (arrow 1). Figure 7b also shows the succession of mineral growth, e.g., the granular crystal (arrow 2) in which a needle has been included, with a subsequent disruption of the growth habit of the grain.

Regardless of the beauty of these crystalline forms, their presence is indicative of a weak bond between the mortar overlay and the concrete substrate. Such crystals can

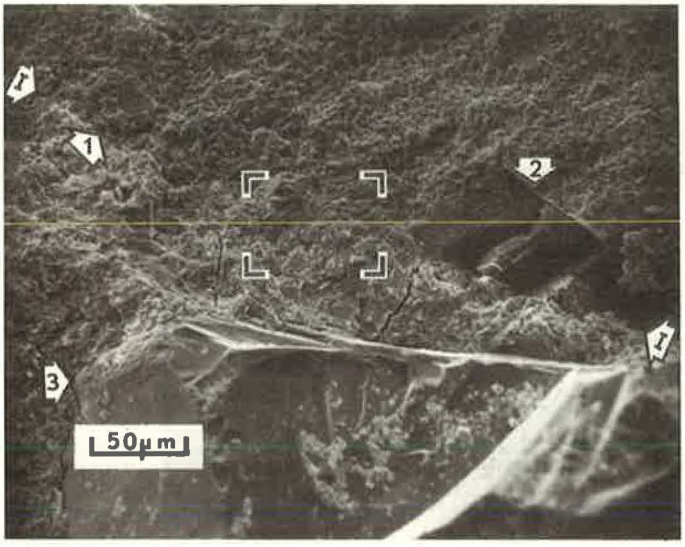

Figure 8a

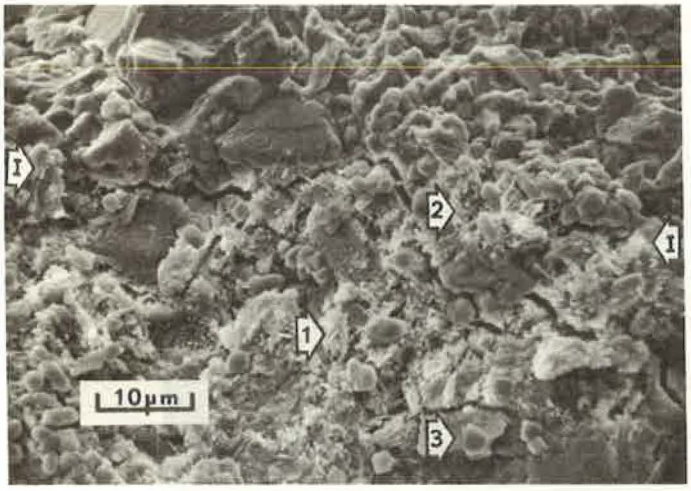

Figure 8b

Figure 8. Standard 3-day composite sample: overlay-substrate interface.

form only in cavities or voids that are filled with liquid or gas. The presence of such cavities or voids decreases the area of contact between the overlay and the substrate. They may be formed either before or after the overlay is applied to the substrate; however, their formation involves materials already present on the surface of the substrate. The absence of both the cavities and the crystals in the sandblasted samples indicates that this or another scarification treatment is necessary to remove these materials.

The next series shows the differences in morphology observed with the standard samples were aged 3, 7, and 14 days. The morphology correlates with an increasing degree of fracture through the concrete substrate, rather than through the mortar overlay or interface. Figures 8 and 9 show the fracture surfaces perpendicular to the overlay-substrate interface, analogous to those shown in Figures 1, 2, and 5. Figure 8 shows the standard sample aged 3 days. Again the interface is marked by arrows, with the substrate above and the overlay below. Figure 8a shows the perimeters of a

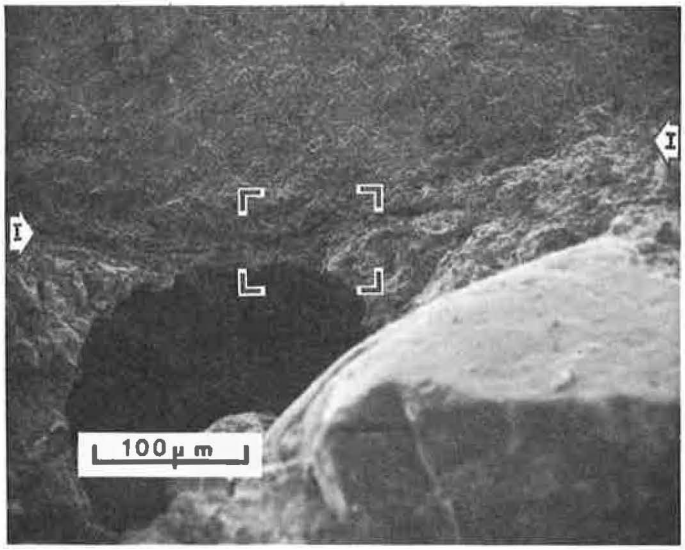

Figure 9a

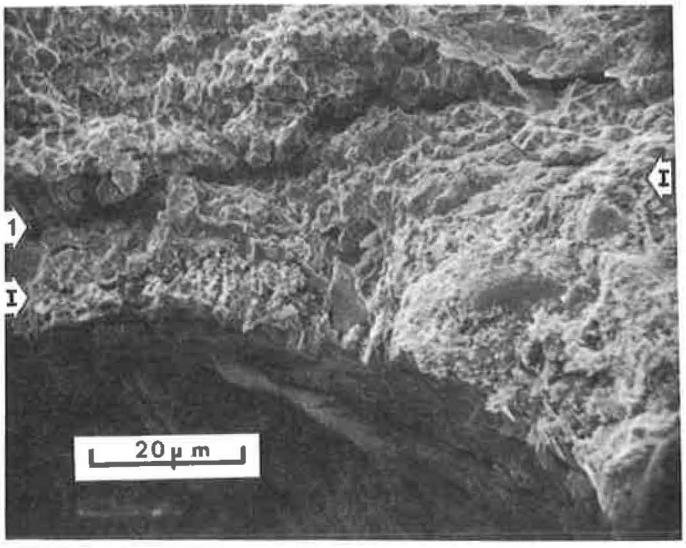

Figure 9b

Figure 9. Standard 7-day composite sample: overlay-substrate interface.

limestone grain (arrow 1) that is flush with the interface. The fractured mass in the limestone grain (arrow 2) is probably calcite because of its rhombohedral form. The large mass (arrow 3) is a sand grain in the overlay mortar. Microcracks can be seen around the peripheries of the sand and limestone grains. Figure 8b clearly shows the microcrack along the mortar side of the limestone-mortar interface. The needle-like crystals lining the channels and fissures (arrow 1) are characteristic of early aging times. The interface can be located only approximately on this scale. A pocket of needles seems to have penetrated the limestone grain (arrow 2), whereas the particle characteristics of the limestone are present in the mortar (arrow 2). Thus, the latex-containing overlay dry-cured for 3 days resembles the control overlay wet-cured for 28 days in that it exhibits needle-filled channels and microcracks on the mortar side of the interface.

Figure 9 shows the standard sample aged 7 days. Again, the interface is marked with arrows and the latex-containing mortar is shown in contact with a limestone grain. These figures show that there are 2 significant differences between 3-day and 7-day aging:

1. The needle-like structures are absent at 7 days (either they have not formed, or they have been covered by the hydration products that formed later); and
2. The microcracks generally follow the overlay-substrate interface but through the substrate adjacent to it, e.g., about 10 μm inside the limestone grain (arrow 1) and the interface is more difficult to locate than in the sample aged 3 days.

The analogous micrographs for the standard sample aged 14 days are not shown because the interface could not be discerned at all at these magnifications. The sample that fractured perpendicularly to the interface showed no microcracks or significant differences in morphology nor any other discontinuities. When this specimen was fractured to simulate the shear bond strength test, the fracture occurred almost entirely throughout the concrete substrate as it did in the actual shear bond test. Thus, the latex-modified overlay became completely integrated with the concrete substrate between 7 and 14 days, under conditions (50 percent RH) that would have severely weakened the ordinary mortar overlay.

Because it is difficult to imagine that a crack present at 3 or 7 days could heal and absent in 14 days, these cracks are assumed to form when the specimen is dried for microscopy under vacuum. The cracks then indicate excessive shrinkage on drying, and they pass through the weakest structures present.

CONCLUSION

The shear bond strength of latex-modified mortar overlays on concrete substrates correlates well with the morphology of the specimens as observed in the scanning electron microscope. The lower bond strength of the control mortar overlay (without latex) correlates with the many microcracks observed throughout the interface between the overlay and the substrate and around the periphery of the sand and limestone grains. The increase in internal and adhesive strength of the latex-modified overlays observed with aging times up to 14 days correlates with the complete integration of the overlay with the substrate, so that the interface can no longer be discerned (it was clearly visible at earlier aging times). The lower bond strengths of the overlay observed when the substrate was not sandblasted before application, correlates with the presence of crystals of various shapes formed in cavities or voids in the interface (neither the crystals nor the voids were observed in the sandblasted sample). These results demonstrate the remarkable utility of the scanning electron microscope for investigating the morphology of portland cement compositions.

REFERENCES

1. Cardone, S. M., Brown, M. G., and Hill, A. A. Latex-Modified Mortar in the Restoration of Bridge Structures. HRB Bull. 260, 1960, pp. 1-13.
2. Shafer, H. H. A Structural Restoration System for Concrete Surfaces. HRB Spec. Rept. 116, abridgment, 1971, pp. 48-50.

3. Siegal, S. Nonparametric Statistics for the Behavioral Sciences. McGraw-Hill, New York, 1956, pp. 75-83.
4. Kimoto, S., and Russ, J. C. The Characteristics and Applications of the Scanning Electron Microscope. American Scientist, Vol. 57, No. 1, 1969, pp. 112-133.